ACS OMEGA

http://pubs.acs.org/journal/acsodf

Article

$MgGd_4Si_3O_{13}:Ce^{3+}$, Mn^{2+}: A Dual-Excitation Temperature Sensor

Aixia Deng, Zilong Wang, Xufeng Zhou, and Wanying Geng*

Cite This: *ACS Omega* 2022, 7, 6481−6487

Read Online

ACCESS | Metrics & More | Article Recommendations | Supporting Information

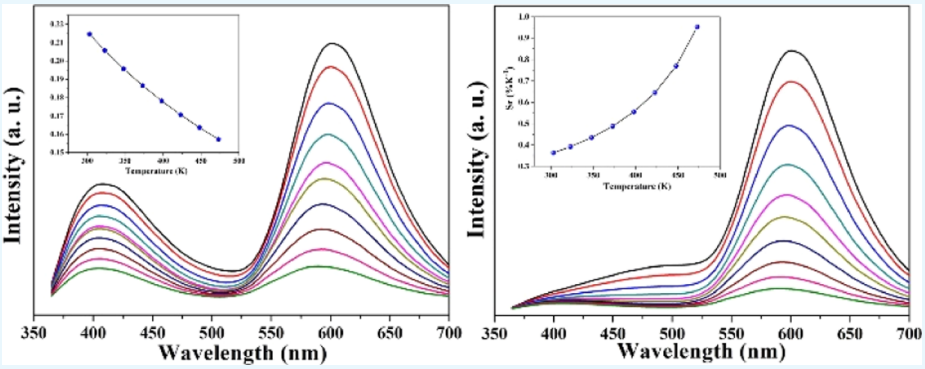

ABSTRACT: A novel apatite-based phosphor $MgGd_4Si_3O_{13}[Mg_2Gd_8(SiO_4)_6O_2]:Ce^{3+}$, Mn^{2+} was designed and successfully synthesized by a solid-state reaction. Based on the different luminescence properties under 298 and 340 nm excitations, its potential application as a dual-excitation luminescent ratiometric thermometer was studied in detail. Under the excitations of 298 and 340 nm, the fluorescent intensity ratio of Ce^{3+} and Mn^{2+} is linearly correlated in the temperature range of 303−473 K. The sensitivity showed an opposite trend with the increase of temperature, and the maximum value was 0.95% K^{-1}. These results indicated that $MgGd_4Si_3O_{13}$: Ce^{3+}, Mn^{2+} can be used as an ideal dual-excitation luminescent ratiometric thermometer.

1. INTRODUCTION

Temperature is one of the important parameters for many physical and chemical reactions. Therefore, it is very significant for many scientific and industrial fields to measure temperature through accurate and effective methods. The fluorescence temperature measurement technology developed based on rare-earth ion-doped inorganic−organic luminescent materials has received wide attention from researchers due to its unique performance, such as realizing noncontact temperature detection, and can work in special environments, such as biological tissues and strong magnetic fields.[1−5] In the early research, the temperature measurement process is mainly based on the change of emission intensity with temperature. However, because the emission intensity is easily affected by external factors such as PH value and luminescence material aggregation, the accuracy of the fluorescence-based temperature sensors based on this principle will also be adversely affected. For the accuracy of temperature, the fluorescence-intensity-ratio-based thermometers which use the emission intensity ratio of two peaks changing with temperature as parameters are developed.[6,7]

Recently, the materials that can be used as temperature sensors have been mainly upconversion nanoparticles (UPNPs). There are also some rare-earth ion-doped complexes and MOF ⊃ dye composites. Compared with UPNPs, MOF ⊃ dye composites often require a complex synthesis process.[8−10] The temperature sensing range of UPNPs is usually excellent; however, the dissatisfactory sensitivity ($CaWO_3:Ho^{3+}/Yb^{3+}$: 3.3−923 K, 0.5% K^{-1}) restricted their applications.[11,12] Downconversion luminescent materials containing two or more luminescent centers have been widely used as LED phosphors. Because of the energy transfer between the luminous centers, the emission intensity of these luminous centers may have different trends with temperature. Based on this performance, some multiple-emission-downconversion luminescent materials show good application potential as temperature sensors.[13−15]

In recent years, many compounds with an apatite structure and same chemical formula of $A_{10}(XO_4)_6Z_2$ have been selected as the host of the luminescent materials because of the superiority of this structure in designing the new materials.[16,17] In our early work, the luminescence properties of Ce^{3+}−Tb^{3+}-doped $MgGd_4Si_3O_{13}[Mg_2Gd_8(SiO_4)_6O_2]$ have been studied in detail.[18] Because the different coordination environments of two cation sites in the crystal, $MgGd_4Si_3O_{13}:Ce^{3+}$ exhibits an

Received: August 28, 2021
Accepted: December 30, 2021
Published: February 19, 2022

obvious difference emission band under different excitation wavelengths (blue emission excited at 298 nm and yellow emission excited at 340 nm). In this work, Ce^{3+}−Mn^{2+}-doped $MgGd_4Si_3O_{13}$ was synthesized to realize the dual-excitation temperature sensors with high sensitivity. The structure and luminescence properties were discussed in detail. Under the excitation of 340 nm, over a wide temperature range (303−473 K), the intensity ratio of Ce^{3+}−Mn^{2+} shows satisfactory linear correlation with the temperature and exhibits a good sensitivity of 0.95% K^{-1}.

2. RESULTS AND DISCUSSION

2.1. Phase Structure of Mn^{2+} Singly and Ce^{3+}, Mn^{2+} Codoped $MgGd_4Si_3O_{13}$. The X-ray diffraction (XRD) patterns of the synthesized $MgGd_{4-x}Si_3O_{13}$:xMn^{2+} ($0.04 \le x \le 0.2$) and $MgGd_{4-x}Si_3O_{13}$:$0.08Ce^{3+}$, xMn^{2+} ($0 \le x \le 0.16$) samples are provided in Figure 1a,b. All the patterns match

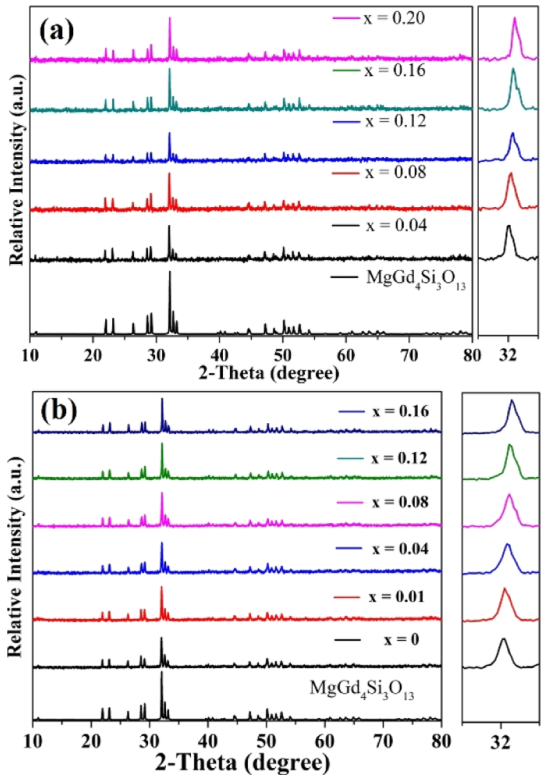

Figure 1. XRD patterns of (a) $MgGd_{4-x}Si_3O_{13}$:xMn^{2+} ($0.04 \le x \le 0.2$) and (b) $MgGd_{4-x}Si_3O_{13}$:$0.08Ce^{3+}$, xMn^{2+} ($0 \le x \le 0.16$) samples.

well with the structural refinement result of $MgGd_4Si_3O_{13}$ and no obvious impurity peak was detected. For both series of samples, the XRD patterns shifted slightly to the large angle direction with the increase in doping concentration, which is due to the change of lattice parameters caused by the different ion radii of Mn^{2+} (0.67 Å, CN = 6; 0.9 Å, CN = 7) and Mg^{2+} (0.72 Å, CN = 6)/Gd^{3+} (1.07 Å, CN = 7).

For the purpose of further studying the occupancy of the doped ions Ce^{3+} and Mn^{2+}, the structural refinement of $MgGd_4Si_3O_{13}$:$0.16Mn^{2+}$ and $MgGd_4Si_3O_{13}$:$0.08Ce^{3+}$, $0.16Mn^{2+}$ is carried out by the Materials Studio program, as shown in Figure 2a,b. The crystal structure parameters of $MgGd_4Si_3O_{13}$:$0.16Mn^{2+}$ and $MgGd_4Si_3O_{13}$:$0.08Ce^{3+}$, $0.16Mn^{2+}$ are given in Table S1, and their atomic coordinates

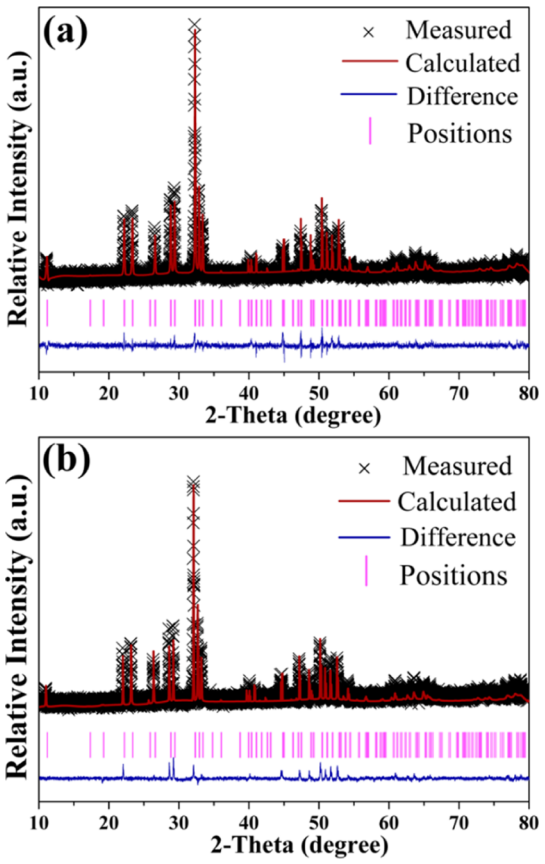

Figure 2. XRD refinement results of (a) $MgGd_4Si_3O_{13}$:$0.16Mn^{2+}$ and (b) $MgGd_4Si_3O_{13}$:$0.08Ce^{3+}$, $0.16Mn^{2+}$.

are given in Tables S2 and S3. It can be seen that $MgGd_4Si_3O_{13}$: $0.16Mn^{2+}$ has a slightly smaller cell volume than $MgGd_4Si_3O_{13}$: $0.08Ce^{3+}$, $0.16Mn^{2+}$. This is because the larger-sized Ce^{3+} (1.07 Å, CN = 7; 1.196 Å, CN = 9) replaces the smaller-sized Gd^{3+} (1.00 Å, CN = 7; 1.107 Å, CN = 9). In addition, the refinement results indicate that Mn^{2+} occupies both Mg/Gd1 and Gd2 sites in the lattice.

2.2. PL Properties. Figure 3a shows the photoluminescence excitation (PLE) spectra of $MgGd_{4-x}Si_3O_{13}$:xMn^{2+} ($0.04 \le x \le 0.2$) samples monitored at 602 nm. Several sharp peaks near 312, 273, and 253 nm belong to the $^8S_{7/2}$−^6P_J, $^8S_{7/2}$−^6I_J, and $^8S_{7/2}$−^6D_J transitions of Gd^{3+}. In our previous work, the transitions of Gd^{3+} also appeared in the PLE spectrum of $MgGd_4Si_3O_{13}$: Tb^{3+}.[18] This phenomenon is caused by the obvious energy transfer mechanism from Gd^{3+} to the doped ions. Except for the transition of Gd^{3+}, other five distinct peaks located at about 343, 367, 409, 414, and 467 nm existing in the excitation spectra are credited to the absorption transitions of Mn^{2+}, respectively. The emission spectra of Mn^{2+}-doped $MgGd_4Si_3O_{13}$ are displayed in Figure 3b, which show a broad red emission around 600 nm under 409 nm excitation. When x increases to 0.16, the emission intensity of the sample reaches the maximum.

In our previous work, the special luminescence properties of Ce^{3+} were discussed. Because Ce^{3+} occupies different coordination environments in $MgGd_4Si_3O_{13}$ (Mg/Gd1 site with nine-coordination and Gd2 site with seven-coordination), under different excitations, Ce^{3+} exhibits distinct emission spectra.[18] The PLE spectra of $MgGd_4Si_3O_{13}$:$0.16Mn^{2+}$ and $MgGd_4Si_3O_{13}$:$0.08Ce^{3+}$, $0.16Mn^{2+}$ and the PL spectra of

https://doi.org/10.1021/acsomega.1c04710
ACS Omega 2022, 7, 6481−6487

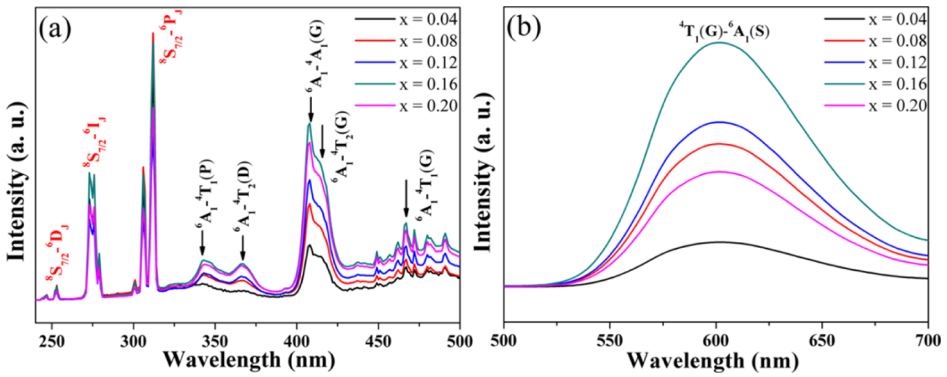

Figure 3. (a) PLE spectra of $MgGd_4Si_3O_{13}$:xMn^{2+} ($0.04 \leq x \leq 0.20$) monitored at 602 nm; (b) the PL spectra of $MgGd_4Si_3O_{13}$: xMn^{2+} ($0.04 \leq x \leq 0.20$) excited at 409 nm.

$MgGd_4Si_3O_{13}$:$0.08Ce^{3+}$ are displayed in Figure 4, respectively. The emission band peaked at 410 nm is attributed to the

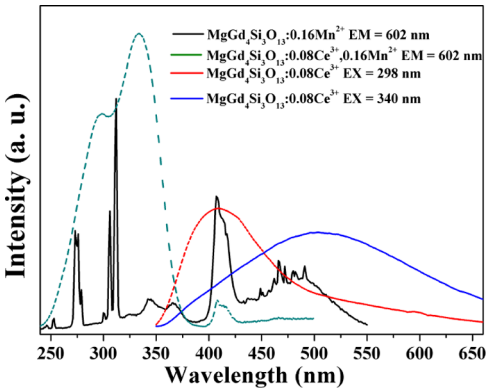

Figure 4. PLE spectra of $MgGd_4Si_3O_{13}$:$0.16Mn^{2+}$ (black) and $MgGd_4Si_3O_{13}$: $0.08Ce^{3+}$, $0.16Mn^{2+}$ (green) monitored at 602 nm. The PL spectra of $MgGd_4Si_3O_{13}$:$0.08Ce^{3+}$ excited at 298 (red) and 340 (blue) nm.

emission of Ce^{3+} occupying the Mg/Gd1 site (Ce1), and the emission band peaked at 505 nm is attributed to the emission of Ce^{3+} occupying the Gd2 site (Ce1). Because the PL spectrum of $MgGd_4Si_3O_{13}$:$0.08Ce^{3+}$ overlaps significantly with the PLE spectrum of $MgGd_4Si_3O_{13}$:$0.16Mn^{2+}$, the energy transfer from the Ce^{3+} to Mn^{2+} ions can be expected in the Ce^{3+} and Mn^{2+} codoped host. In addition, the 4f−5d transition of Ce^{3+} is observed in the excitation spectrum of $MgGd_4Si_3O_{13}$:$0.08Ce^{3+}$, $0.16Mn^{2+}$ (the green line in Figure 4) monitoring at 602 nm emission (the emission of Mn^{2+}), which demonstrates that there is an effective energy transfer effect between Ce^{3+} and Mn^{2+}.

In order to study the energy transfer from Ce^{3+} to Mn^{2+}, a series of $MgGd_4Si_3O_{13}$:$0.08Ce^{3+}$, xMn^{2+} ($0 \leq x \leq 0.16$) samples have been prepared. Figure 5a,b displays the PL spectra excited at 298 and 340 nm, respectively. It can be seen that with the increase of Mn^{2+} concentration, the emission intensity of Ce^{3+} decreases monotonically, which can be used as the evidence of energy transfer between Ce^{3+} and Mn^{2+}. Therefore, according to the different emission positions of Ce^{3+} and Mn^{2+}, the color can be adjusted from blue to red (as shown in Figure S1). Figure S2 displays the decay curves of Ce^{3+}, and based on the Dexter's and Reisfeld's theories and decay curves, the dominant energy transfer mechanism from Ce^{3+} to Mn^{2+} was identified as a dipole−quadrupole interaction (as shown in Figure S3).[19−22]

2.3. Thermal Stability and Ratiometric Temperature Sensing. The temperature-dependent PL spectra of $MgGd_4Si_3O_{13}$:$0.08Ce^{3+}$excited at 298 and 340 nm are shown in Figure 6a,b, respectively. The luminescence intensities of Ce^{3+}decrease obviously with the increase of temperature. Moreover, when the temperature rises to 200 °C, the emission band at 505 nm disappears, while the band at 410 nm occurs. All these changes have been shown in the inset of Figure 6b, which indicates that the thermal stability of Ce1 and Ce2 is obviously different. Generally, the Ce^{3+} located at the rigid host lattice is expected to have good thermal stability with a narrow emission band.[23−25] By comparing the emission spectra of Ce1 and Ce2, it is found that the half-height width of Ce1 is

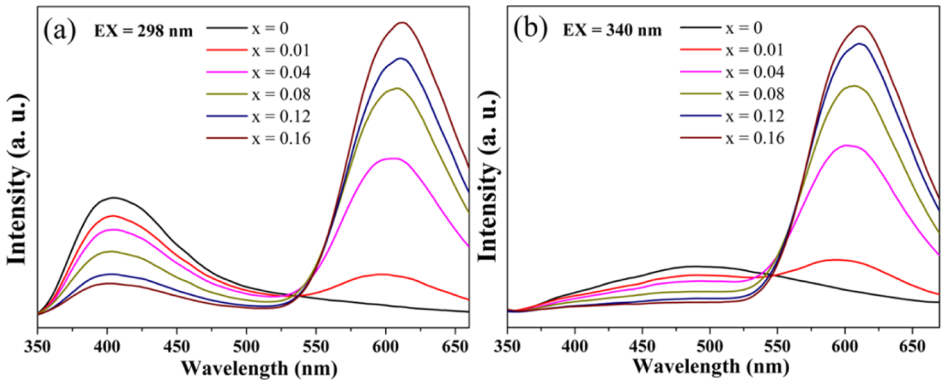

Figure 5. PL spectra of $MgGd_4Si_3O_{13}$:$0.08Ce^{3+}$, xMn^{2+} ($0 \leq x \leq 0.16$) excited at (a) 298 and (b) 340 nm.

https://doi.org/10.1021/acsomega.1c04710
ACS Omega 2022, 7, 6481−6487

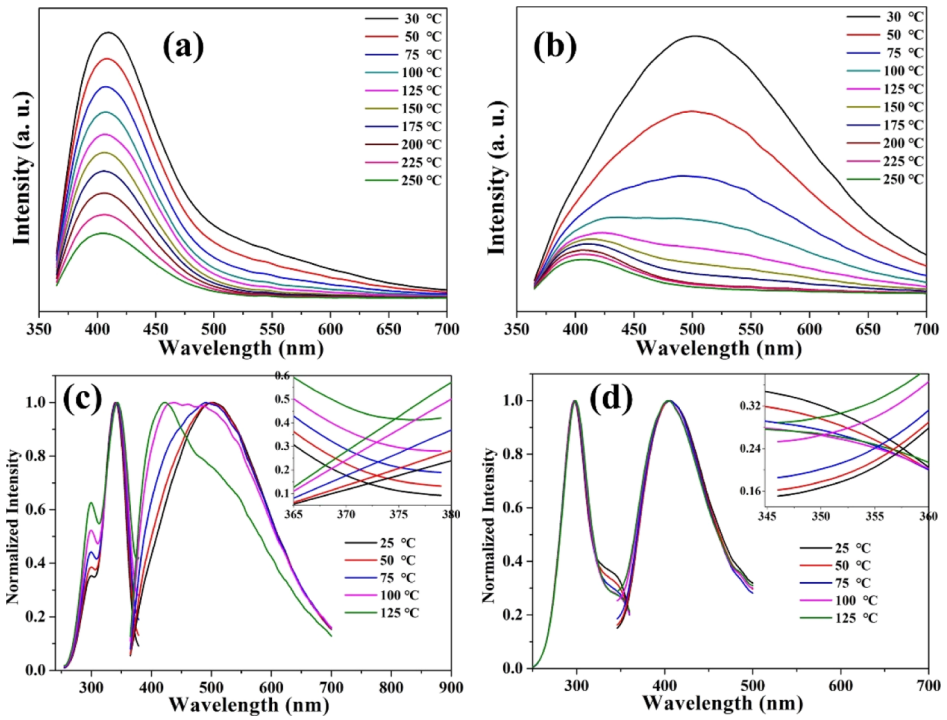

Figure 6. Temperature-dependent PL spectra of $MgGd_4Si_3O_{13}$:0.08Ce^{3+} excited at (a) 298 and (b) 340 nm, respectively. The normalized PLE and PL spectra of $MgGd_4Si_3O_{13}$:0.08Ce^{3+} excited at (c) 298 and (d) 340 nm with the temperature increased from 25 to 125 °C, and the insets show the enlarged view of the spectral overlap region.

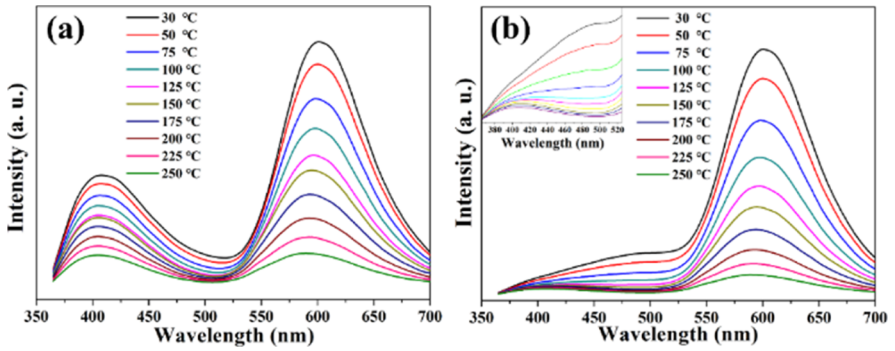

Figure 7. Temperature-dependent PL spectra of $MgGd_4Si_3O_{13}$:0.08Ce^{3+}, 0.16 Mn^{2+} excited at (a) 298 and (b) 340 nm, respectively. The inset is the enlarged view of the spectra in the range of 360−520 nm.

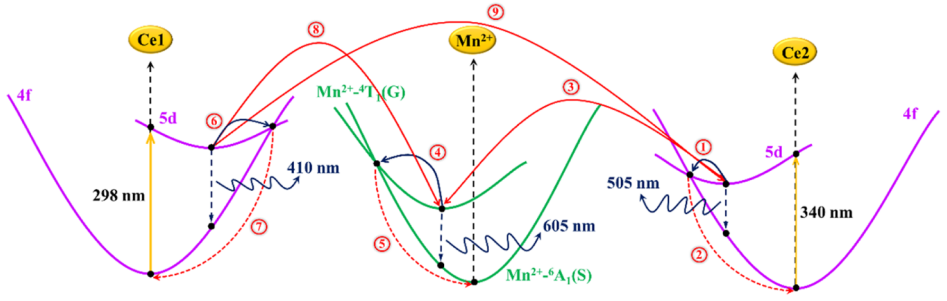

Figure 8. Configurational coordinate diagram of the ground and excited state of Ce1, Ce2, and Mn^{2+}.

significantly smaller than that of Ce2, which indicates that the Mg/Gd1 site shows better structural rigidity than the Gd2 site. Therefore, Ce1 has better thermal stability than Ce2.The obvious difference in thermal stability between Ce1 and Ce2 is attributed to the different structural rigidities of Mg/Gd1 and Gd2 sites. Due to the stronger rigidity of the Mg/Gd1 site, Ce1 exhibits a relatively narrower emission band and better thermal stability. The results of normalized spectra (shown in Figure 6c,d) also indicate that with the increase of temperature, the excitation and emission spectra of Ce2 appear more obvious broadening, indicating that Ce2 is more obviously affected by phonons. The spectral broadening results show that after the

https://doi.org/10.1021/acsomega.1c04710
ACS Omega 2022, 7, 6481−6487

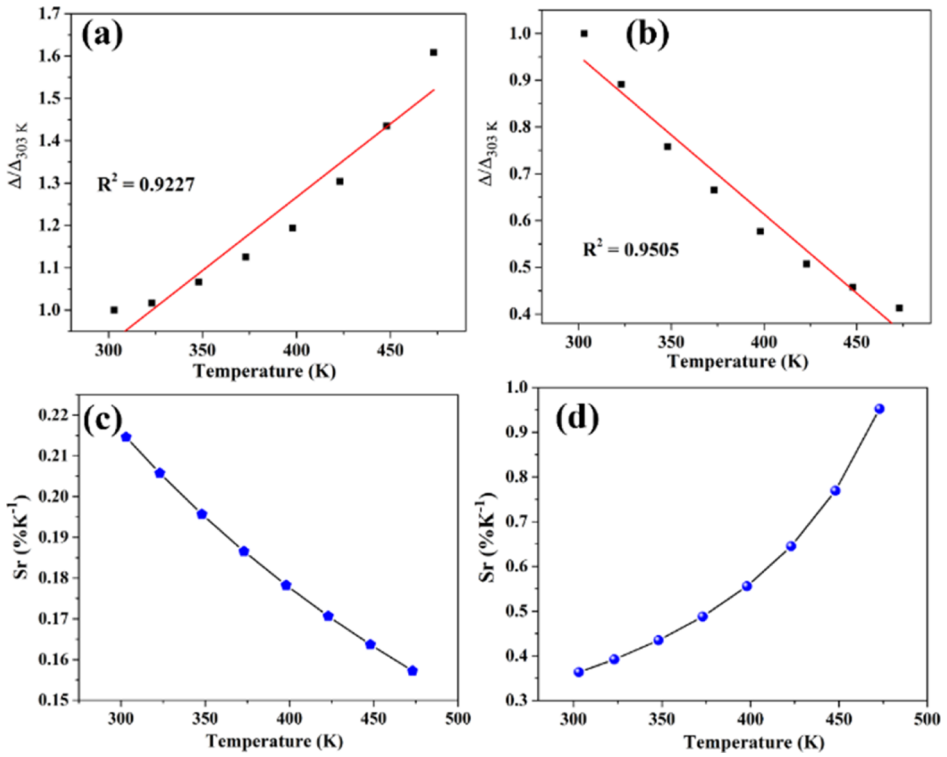

Figure 9. (a,b) Temperature-dependent intensity ratio (Δ/Δ_{303} K) and linearly fitted curve under 298 and 340 nm excitation; (c,d) Variation of relative sensitivity with temperature under 298 and 340 nm excitation.

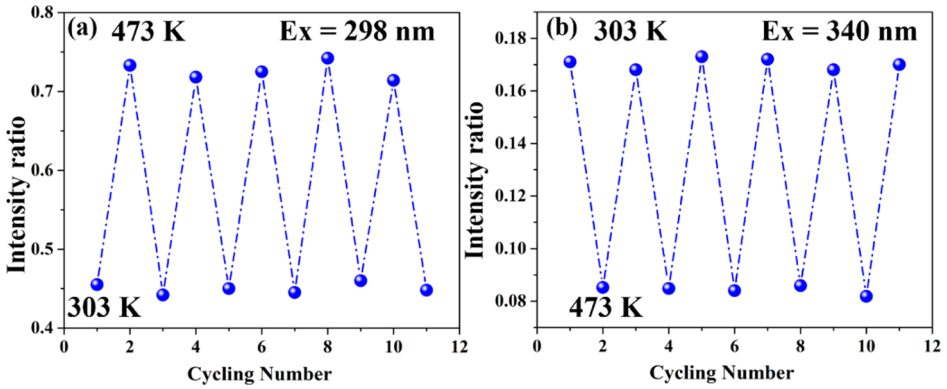

Figure 10. Cyclic heating test of $MgGd_4Si_3O_{13}$:0.08Ce^{3+}, 0.16Mn^{2+} between 303 and 473 K excited at (a) 298 and (b) 340 nm, respectively.

electrons of Ce2 are excited to the 5d level, they are more likely to return to the 4f level in a radiation-free way through cross-relaxation, resulting in a more obvious emission intensity reduction.

The temperature-dependent PL spectra of $MgGd_4Si_3O_{13}$:0.08Ce^{3+}, 0.16 Mn^{2+} excited at 298 and 340 nm are shown in Figure 7a,b, respectively. The luminescence intensities of Ce^{3+} and Mn^{2+} decrease obviously with the increase of temperature. To further investigate the thermal quenching phenomenon of the $MgGd_4Si_3O_{13}$:0.08Ce^{3+}, 0.16 Mn^{2+} sample, a configurational coordinate diagram based on the spectra is shown in Figure 8.[26−28] When $MgGd_4Si_3O_{13}$:Ce^{3+}, Mn^{2+} was excited under 340 nm excitation, some of the excited electrons jumped to the ground state and produced the yellow light emission, and some of them back to the ground state with nonradiation relaxation by passing through the intersection of the ground state and the excited state, causing the loss of luminescence intensity (① and ②). At the same time, some excited electrons transfer energy to the electrons of Mn^{2+}, making the electrons of Mn^{2+} transition to the excited state (③). Similarly, some of these electrons transition back to the ground state to produce red light emission, and some of them relax to the ground state without radiation through the intersection of the ground state and the excited state (④ and ⑤). When the material is excited at 298 nm, the excited electrons of Ce1 will not only produce the blue emission and nonradiation relaxation (⑥ and ⑦) but also transfer energy to Ce2 and Mn^{2+} (⑧ and ⑨). Therefore, under 298 nm excitation, the process ① to ⑤ and the emission of Ce2 and Mn^{2+} will also occur.

Based on the above discussion, we can take the luminescence intensity ratio of Ce^{3+} and Mn^{2+} ($\Delta = I_{Ce_{3+}}/I_{Mn_{2+}}$) as a temperature measurement parameter. Figure 9a,b shows the changes of the luminescence intensity ratio at different temperatures when $MgGd_4Si_3O_{13}$:0.08Ce^{3+}, 0.16

https://doi.org/10.1021/acsomega.1c04710
ACS Omega 2022, 7, 6481−6487

Mn^{2+} is excited at 298 and 340 nm, respectively. The Δ values are normalized to the Δ_{303K} value (Δ value at room temperature). It can be seen that the normalized Δ values are linearly correlated in the range of 303−473 K. According to the linear fitting results, the relative sensitivity (Sr) can be calculated according to the following formula[29]

$$\mathrm{Sr} = \left|\frac{\partial\Delta/\partial T}{\Delta}\right|$$

where Δ is the intensity ratio and T is the temperature. Figure 9c,d exhibits the variation in the Sr values at different temperatures. Under different excitations, the sensitivity shows different trends with the temperature. Under 298 nm excitation, the Sr decreased with the increase of temperature, and the maximum value was 0.21% K^{-1}. Under 340 nm excitation, the Sr increased with the increase of temperature, and the maximum value was 0.95% K^{-1}. Besides, the five-time cyclic heating test of $MgGd_4Si_3O_{13}$:0.08Ce^{3+}, 0.16Mn^{2+} between 303 and 473 K is given in Figure 10. The $MgGd_4Si_3O_{13}$:0.08Ce^{3+}, 0.16Mn^{2+} sample showed that the recycling performance and the change of fluorescence intensity ratio are less than 5% after five cycling steps. The Sr value and temperature range of $MgGd_4Si_3O_{13}$:0.08Ce^{3+}, 0.16Mn^{2+} and some Ce^{3+}−Mn^{2+} codoped thermometers are provided in Table 1.[14,30,31] Comparing with our previous report [$NaBaSc(BO_3)_2$: Ce^{3+}, Mn^{2+}], the sensitivity of $MgGd_4Si_3O_{13}$: Ce^{3+}, Mn^{2+} is not outstanding, but it still has advantages over other phosphors. These results showed that $MgGd_4Si_3O_{13}$: Ce^{3+}, Mn^{2+} phosphors could be used as a high-sensitivity optical thermometer.

Table 1. Sr Values and Temperature Range of $MgGd_4Si_3O_{13}$:0.08Ce^{3+}, 0.16Mn^{2+} and Some Ce^{3+}−Mn^{2+} Codoped Thermometers

material	Sr (% K^{-1})	temperature range (K)	references
$MgGd_4Si_3O_{13}$:Ce^{3+}, Mn^{2+}	0.21 (298 nm)	300−473	this work
	0.95 (340 nm)	303−473	
$(Ca,Sr)_{10}Li(PO_4)_7$:Ce^{3+}, Mn^{2+}	0.4	293−473	30
$NaMgBO_3$: Ce^{3+}, Mn^{2+}	0.69	293−473	31
$NaBaSc(BO_3)_2$: Ce^{3+}, Mn^{2+}	3.16	298−473	14

3. CONCLUSIONS

In summary, a novel apatite dual-excitation luminescent ratiometric thermometer $MgGd_4Si_3O_{13}$: Ce^{3+}, Mn^{2+} was successfully synthesized via the solid-state method. The energy transfer between Ce^{3+} and Mn^{2+} was discussed in detail. The luminescent properties of Mn^{2+} and the temperature-dependent luminescent properties of $MgGd_4Si_3O_{13}$: Ce^{3+}, Mn^{2+} have been investigated. Under the excitations of 298 and 340 nm, the fluorescent intensity ratio of Ce^{3+} and Mn^{2+} is linearly related to the temperature in the range of 303−473 K with high sensitivity of 0.95% K^{-1}. The above results indicate that $MgGd_4Si_3O_{13}$: Ce^{3+}, Mn^{2+} can serve as a good candidate material for luminescent ratiometric thermometry.

4. Experimental Section. *4.1. Preparation of Materials.* All samples in our work were synthesized by the solid-state reaction. The starting materials were Gd_2O_3 (99.99%), $MnCO_3$ (99.99%), CeO_2 (99.99%), H_2SiO_3 (A.R.), and MgO (A.R.). These materials were used as raw materials without any further purification. After been mixed well in agate mortar, these ingredients were calcinated at 1480 °C in a reducing atmosphere of 20% H_2−80% N_2 for 6 h.

4.2. Characterization. The phase structures of the obtained samples were tested by a Rigaku D/Max-2400 diffractometer with Ni-filtered Cu Kα radiation. The PL properties (PL, PLE spectra, and PL decay curves) were obtained by a FLS-920T fluorescence spectrophotometer equipped with Xe and nF900 ns Flashlamp source. All the measurements were performed at room temperature. The temperature-dependent emission was tested combined with the heating apparatus (TAP-02).

■ ASSOCIATED CONTENT

Supporting Information

The Supporting Information is available free of charge at https://pubs.acs.org/doi/10.1021/acsomega.1c04710.

CIE chromaticity diagram for $MgGd_4Si_3O_{13}$:0.08Ce^{3+}, x Mn^{2+} ($0 \le x \le 0.16$) excited at 298 and 340 nm; decay curves for Ce^{3+} in $MgGd_4Si_3O_{13}$:0.08Ce^{3+}, $x$$Mn^{2+}$ ($0 \le x \le 0.16$); fluorescence lifetime of Ce^{3+} and the energy transfer efficiency from Ce^{3+} to Mn^{2+} as a function of Mn^{2+} concentration under 298 and 340 nm excitations; ratio I_0/I of Ce^{3+} on $C_{Mn}^{6/3}$, $C_{Mn}^{8/3}$, and $C_{Mn}^{10/3}$ excited at 298 and 340 nm; crystal structural data and lattice parameters of $MgGd_4Si_3O_{13}$: 0.16Mn^{2+} and $MgGd_4Si_3O_{13}$:0.08Ce^{3+}, 0.16Mn^{2+}; and atomic coordinates for $MgGd_4Si_3O_{13}$:0.16Mn^{2+} and $MgGd_4Si_3O_{13}$:0.08Ce^{3+}, 0.16Mn^{2+} (PDF)

■ AUTHOR INFORMATION

Corresponding Author

Wanying Geng − *School of Material Science and Engineering, Liaocheng University, Liaocheng 252000, China;* orcid.org/0000-0002-9730-0450; Email: gengwanying@lcu.edu.cn

Authors

Aixia Deng − *School of Material Science and Engineering, Liaocheng University, Liaocheng 252000, China*

Zilong Wang − *School of Material Science and Engineering, Liaocheng University, Liaocheng 252000, China*

Xufeng Zhou − *School of Material Science and Engineering, Liaocheng University, Liaocheng 252000, China*

Complete contact information is available at: https://pubs.acs.org/10.1021/acsomega.1c04710

Notes

The authors declare no competing financial interest.

■ ACKNOWLEDGMENTS

We acknowledge the financial support from the National Natural Science Foundation of China (grant no. 12004148), PhD early development program of Liaocheng University (318051936), and Innovation Team of Higher Educational Science and Technology Program in Shandong Province (no. 2019KJA025).

■ REFERENCES

(1) Dong, B.; Cao, B.; He, Y.; Liu, Z.; Li, Z.; Feng, Z. Temperature sensing and in vivo imaging by molybdenum sensitized visible

upconversion luminescence of rare - earth oxides. *Adv. Mater.* **2012**, *24*, 1987−1993.
(2) Chen, D.; Wan, Z.; Zhou, Y.; Zhou, X.; Yu, Y.; Zhong, J.; Ding, M.; Ji, Z. Dual-phase glass ceramic: structure, dual-modal luminescence, and temperature sensing behaviors. *ACS Appl. Mater. Interfaces* **2015**, *7*, 19484−19493.
(3) Chen, D.; Wan, Z.; Zhou, Y. Optical spectroscopy of Cr^{3+}-doped transparent nano-glass ceramics for lifetime-based temperature sensing. *Opt. Lett.* **2015**, *40*, 3607−3610.
(4) Gao, Y.; Huang, F.; Lin, H.; Zhou, J.; Xu, J.; Wang, Y. A novel optical thermometry strategy based on diverse thermal response from two intervalence charge transfer states. *Adv. Funct. Mater.* **2016**, *26*, 3139−3145.
(5) Skripka, A.; Benayas, A.; Marin, R.; Canton, P.; Hemmer, E.; Vetrone, F. Double rare-earth nanothermometer in aqueous media: opening the third optical transparency window to temperature sensing. *Nanoscale* **2017**, *9*, 3079−3085.
(6) Cui, Y.; Xu, H.; Yue, Y.; Guo, Z.; Yu, J.; Chen, Z.; Gao, J.; Yang, Y.; Qian, G.; Chen, B. A luminescent mixed-lanthanide metal−organic framework thermometer. *J. Am. Chem. Soc.* **2012**, *134*, 3979−3982.
(7) Rao, X.; Song, T.; Gao, J.; Cui, Y.; Yang, Y.; Wu, C.; Chen, B.; Qian, G. A highly sensitive mixed lanthanide metal−organic framework self-calibrated luminescent thermometer. *J. Am. Chem. Soc.* **2013**, *135*, 15559−15564.
(8) Jethi, L.; Krause, M. M.; Kambhampati, P. Toward ratiometric nanothermometry via intrinsic dual emission from semiconductor nanocrystals. *J. Phys. Chem. Lett.* **2015**, *6*, 718−721.
(9) Yang, Y.; Chen, L.; Jiang, F.; Yu, M.; Wan, X.; Zhang, B.; Hong, M. A family of doped lanthanide metal−organic frameworks for wide-range temperature sensing and tunable white light emission. *J. Mater. Chem. C* **2017**, *5*, 1981−1989.
(10) Cui, Y.; Song, R.; Yu, J.; Liu, M.; Wang, Z.; Wu, C.; Yang, Y.; Wang, Z.; Chen, B.; Qian, G. Dualemitting MOF⊃Dye composite for ratiometric temperature sensing. *Adv. Mater.* **2015**, *27*, 1420−1425.
(11) Xu, W.; Zhao, H.; Li, Y.; Zheng, L.; Zhang, Z.; Cao, W. Optical temperature sensing through the upconversion luminescence from Ho^{3+}/Yb^{3+} codoped $CaWO_4$. *Sens. Actuators, B* **2013**, *188*, 1096−1100.
(12) Li, D.; Wang, Y.; Zhang, X.; Yang, K.; Liu, L.; Song, Y. Optical temperature sensor through infrared excited blue upconversion emission in Tm^{3+}/Yb^{3+} codoped Y_2O_3. *Opt. Commun.* **2012**, *285*, 1925−1928.
(13) Zhou, X.; Geng, W.; Ding, J.; Zhao, Z.; Wang, Y. $Ca_2Na_2La_6(SiO_4)_4(PO_4)_2O$: Eu^{2+}/Eu^{3+}: A visual dual-emitting fluorescent ratiometric temperature sensor. *J. Am. Ceram. Soc.* **2019**, *102*, 5443−5453.
(14) Geng, W.; Zhou, X.; Ding, J.; Wang, Y. Density-functional theory calculations, luminescence properties and fluorescence ratiometric thermo-sensitivity for a novel borate based red phosphor: $NaBaSc(BO_3)_2$: Ce^{3+}, Mn^{2+}. *J. Mater. Chem. C* **2019**, *7*, 1982−1990.
(15) Yan, B.; Wei, Y.; Wang, W.; Fu, M.; Li, G. Red-tunable LuAG garnet phosphors via $Eu^{3+}\rightarrow Mn^{4+}$ energy transfer for optical thermometry sensor application. *Inorg. Chem. Front.* **2021**, *8*, 746−757.
(16) Tian, Y.; Wei, Y.; Zhao, Y.; Quan, Z.; Li, G.; Lin, J. Photoluminescence tuning of $Ca_5(PO_4)_3Cl$: Ce^{3+}/Eu^{2+}, Tb^{3+}/Mn^{2+} phosphors: structure refinement, site occupancy, energy transfer and thermal stability. *J. Mater. Chem. C* **2016**, *4*, 1281−1294.
(17) Zhou, X.; Geng, W.; Ding, J.; Wang, Y.; Wang, Y. Structure, bandgap, photoluminescence evolution and thermal stability improved of Sr replacement apatite phosphors $Ca_{10-x}Sr_x(PO_4)_6F_2$:Eu^{2+}(x= 4, 6, 8). *Dyes Pigm.* **2018**, *152*, 75−84.
(18) Zhou, X.; Zhang, Z.; Wang, Y. Ce^{3+} and Tb^{3+} singly-and co-doped $MgGd_4Si_3O_{13}$ for ultraviolet light emitting diodes and field emission displays. *J. Mater. Chem. C* **2015**, *3*, 3676−3683.
(19) Fan, F.; Zhao, L.; Shang, Y.; Liu, J.; Chen, W.; Li, Y. Thermally stable double-perovskite Ca_3TeO_6: Eu^{3+} red-emitting phosphors with high color purity. *J. Lumin.* **2019**, *211*, 14−19.
(20) Lahoz, F.; Martín, I. R.; Méndez-Ramos, J.; Núñez, P. Dopant distribution in a Tm^{3+}-Yb^{3+} codoped silica based glass ceramic: an infrared-laser induced upconversion study. *J. Chem. Phys.* **2004**, *120*, 6180−6190.
(21) Blasse, G. Energy transfer in oxidic phosphors. *Phys. Lett. A* **1968**, *28*, 444−445.
(22) Blasse, G.; Grabmaier, B. C. *Luminescent Materials*; SpringerVerlag: Berlin, Germany, 1994.
(23) Wang, Y.; Ding, J.; Wang, Y.; Zhou, X.; Cao, Y.; Ma, B.; Li, J.; Wang, X.; Seto, T.; Zhao, Z. Structural design of new Ce^{3+}/Eu^{2+}-doped or co-doped phosphors with excellent thermal stabilities for WLEDs. *J. Mater. Chem. C* **2019**, *7*, 1792−1820.
(24) Hu, T.; Molokeev, M. S.; Xia, Z.; Zhang, Q. Aliovalent substitution toward reinforced structural rigidity in Ce^{3+}-doped garnet phosphors featuring improved performance. *J. Mater. Chem. C* **2019**, *7*, 14594−14600.
(25) Qiao, J.; Zhao, J.; Liu, Q.; Xia, Z. Recent advances in solid-state LED phosphors with thermally stable luminescence. *J. Rare Earths* **2019**, *37*, 565−572.
(26) Ji, X.; Zhang, J.; Li, Y.; Liao, S.; Zhang, X.; Yang, Z.; Wang, Z.; Qiu, Z.; Zhou, W.; Yu, L.; Lian, S. Improving Quantum Efficiency and Thermal Stability in Blue-Emitting $Ba_{2-x}Sr_xSiO4$: Ce^{3+} Phosphor via Solid Solution. *Chem. Mater.* **2018**, *30*, 5137−5147.
(27) Zhang, Q.; Wang, X.; Tang, Z.; Wang, Y. A K3ScSi2O7: Eu^{2+} based phosphor with broad-band NIR emission and robust thermal stability for NIR pc-LEDs. *Chem. Commun.* **2020**, *56*, 4644−4647.
(28) Qu, M.; Zhang, X.; Mi, X.; Liu, Q.; Bai, Z. Novel color tunable garnet phosphor of Tb^{3+} and Eu^{3+} co-doped $Ca_2YZr_2Al_3O_{12}$ with high thermal stability via energy transfer. *J. Alloys Compd.* **2020**, *828*, 154398.
(29) McLaurin, E. J.; Bradshaw, L. R.; Gamelin, D. R. Dual-emitting nanoscale temperature sensors. *Chem. Mater.* **2013**, *25*, 1283−1292.
(30) Zhang, X.; Xu, J.; Guo, Z.; Gong, M. Luminescence and energy transfer of dual-emitting solid solution phosphors $(Ca, Sr)_{10}Li(PO_4)_7$: Ce^{3+}, Mn^{2+} for ratiometric temperature sensing. *Ind. Eng. Chem. Res.* **2017**, *56*, 890−898.
(31) Song, J.; Zhao, W.; Zhang, H.; Liu, Y.; Huang, H.; Yang, H.; Zhang, H.; Zhong, J. Energy transfer and ratiometric Temperature sensing based on the dual-emitting $NaMgBO_3$: Ce^{3+}, Mn^{2+} phosphor. *J. Lumin.* **2021**, *232*, 117858.

https://doi.org/10.1021/acsomega.1c04710
ACS Omega 2022, 7, 6481−6487